Available online at www.sciencedirect.com
ScienceDirect
Tetrahedron
Tetrahedron 64 (2008) 2126–2133
www.elsevier.com/locate/tet

A matrix isolation study on Ac–L-Pro–NH_2: a frequent structural element of β- and γ-turns of peptides and proteins

Gábor Pohl [a], András Perczel [a,b], Elemér Vass [c], Gábor Magyarfalvi [d], György Tarczay [d,*]

[a] *Structural Chemistry and Biology Laboratory, Institute of Chemistry, Eötvös University, PO Box 32, H-1518, Budapest 112, Hungary*
[b] *Protein Modelling Group MTA-ELTE, Institute of Chemistry, Eötvös University, PO Box 32, H-1518, Budapest 112, Hungary*
[c] *Laboratory for Chiroptical Structure Analysis, Institute of Chemistry, Eötvös University, PO Box 32, H-1518, Budapest 112, Hungary*
[d] *Laboratory of Molecular Spectroscopy, Institute of Chemistry, Eötvös University, PO Box 32, H-1518, Budapest 112, Hungary*

Received 8 September 2007; received in revised form 19 November 2007; accepted 14 December 2007
Available online 23 December 2007

This article is dedicated to celebrate 80th birthday of Professor Csaba Szántay

Abstract

The fine tuned flexibility of peptides and proteins is one of their key features to achieve full bioactivity. Proline diamides are inherently the most rigid natural peptide models, but they still have a potential to adopt several backbone and side-chain conformers. It has been tried to spell out the residual conformational flexibility of Ac–L-Pro–NH_2 using matrix isolation IR and VCD spectroscopy in Ar and Kr matrices. Spectra were analyzed by the help of quantum chemical calculations. The spectra are dominated by the transitions of the $t\gamma_L+$ conformer, furthermore trace amounts of the $c\alpha_L+$ conformer are also present. Another low-energy conformer, $t\gamma_L-$, cannot be identified in the spectra, which was interpreted as it converts to the lowest energy $t\gamma_L+$ form through a low-energy barrier during the deposition of the sample onto the cold window. Our results confirm that proline can act as a conformational lock, since the backbone predominantly adapts to the $t\gamma_L$ structure.

1. Introduction

Short linear polypeptides have the potential to adopt hundreds if not thousands of conformers. N- and C-protected amino acid residues are claimed to be promising conformational models of the amino acid residues within peptides and proteins. Out of the 20 natural amino acid residues proline is the only one whose side chain is covalently bonded to the nitrogen of the peptide backbone by forming a pyrrolidine ring. This unique structural feature has an important role in stabilizing segments of proteins, as it imposes a constraint on the backbone conformation of the subunit.[1] The limited internal plasticity of proline is used by evolution to establish local backbone rigidity. The rigidity of the C(O)–N–C^{α}–C(O) torsion angle, ϕ, makes proline both an α-helix and a β-sheet breaker structural element of the polypeptide chain and favors the formation of polyproline helices. Furthermore, unlike other amino acids, the amide bond at the N-terminal of proline can easily isomerize between cis and trans forms due to the imide type nitrogen, which weakens the conjugation. Besides backbone conformations and cis–trans forms the conformational space has a third dimension when L-proline containing model peptides are considered. This is because the pyrrolidine ring is not planar, therefore ring-puckering conformers come to the scene.[2]

Proline diamide derivatives, such as *N*-formylproline amide (For–L-Pro–NHMe), *N*-acetylproline amide (Ac–L-Pro–NH_2), *N*-acetylproline-*N*′-methyl amide (Ac–L-Pro–NHMe), and *N*-acetylproline-*N*′,*N*′-dimethyl amide (Ac–L-Pro–NMe_2) can be considered as suitable structural models of the proline units embedded in a polypeptide chain. Therefore, these model peptides have been extensively studied both by

* Corresponding author.
E-mail address: tarczay@chem.elte.hu (G. Tarczay).

0040-4020/$ - see front matter © 2008 Elsevier Ltd. All rights reserved.
doi:10.1016/j.tet.2007.12.037

spectroscopic and theoretical methods. In general in these experimental studies four types of conformers were considered, trans and cis isomers with and without H-bonding.

Infrared (IR)[3–12] and vibrational circular dichroism (VCD)[13–15] experiments revealed that both cis and trans isomers of proline diamides are present in each solvent. In apolar solvents the trans γ-turn conformer is the most abundant. The population of the cis isomer and trans polyproline-II helix conformer (denoted as ε_L in this study) was found to increase with solvent polarity. The estimated amount of the cis form was ~5% in CCl_4,[16] ~20% in $CDCl_3$,[8,12] and 12.5% in CD_2Cl_2,[11] respectively. Recent 2D IR spectroscopic studies[17–24] confirmed the conclusions outlined above. These studies have revealed that a simple continuum solvent model is unsuitable to explain the conformational distributions, but specific solute–solvent interactions, such as hydrogen bonding and steric hindrance have to be considered to understand the structure and the conformational equilibrium in solvents.[24]

In agreement with the IR investigations NMR studies[6,11,12,25–29] have also proved that the ratio of the cis isomer is higher in polar than in apolar solvents. The estimated amount of the cis isomer was found to be 0–11% in CCl_4,[27] 6–19% in $CDCl_3$,[7,12,27] ~27% in $(CD_3)_2CO$,[27] and ~26% in D_2O,[27] respectively. It has been found that in apolar solvents the trans isomer mostly exhibits a γ-turn structure with an intramolecular hydrogen bond, while the cis isomer tends to form oligomers by intermolecular hydrogen bonds. As expected the cis/trans ratio has been found to be sensitive to temperature and concentration in nonpolar solvents. In contrast to this, in polar solvents, both the cis and trans isomers exist as monomers due to the strong interaction with solvent molecules.[27] The barrier height of the cis–trans isomerization was determined to be 75 kJ mol^{-1}.

Ring puckering and cis–trans isomerization of proline derivatives were also investigated by NMR spectroscopy. It has been found that the two conformers (*exo* and *endo*, or + and − as denoted in this study) are equally populated.

In order to explain the experimental results, numerous theoretical calculations were also carried out on proline dipeptides, including molecular mechanics (MM),[30–33] semiempirical,[34–39] ab initio,[2,38–48] and density functional theory (DFT)[41–49] methods. Most recent calculations located three trans and four cis conformers on the Hartree–Fock potential energy surface (PES) of Ac-L-Pro–NH_2[39,47] and For–L-Pro–NH_2,[2] while only two cis and four trans conformers were found by DFT methods.[47] In accordance with experimental results in apolar solvents, the trans γ-turn conformation was found to be the most stable. Solvent model calculations have shown that the amount of the different cis isomers and the polyproline-II form increases with solvent polarity.[42,44,45,48] Furthermore, in agreement with experimental findings ab initio calculations have also confirmed that the energy difference of the corresponding + and − ring-puckering forms is about 2–8 kJ mol^{-1}, and the barrier heights from the higher energy puckering forms to the lower energy ones are in the order of 2–14 kJ mol^{-1}.[2,39,42]

The purpose of the present study is to investigate Ac–L-Pro–NH_2 in low-temperature Ar and Kr matrices, using matrix isolation infrared (MI-IR) and the matrix isolation VCD (MI-VCD) spectroscopy. The obtained experimental results can directly be compared to computational results on isolated molecules testing the reliability of the theoretical methods.

2. Experimental details

2.1. General

Ac–L-Pro–NH_2 (purity of >99%) was obtained from Bachem. The sample was evaporated into the vacuum chamber by using a home built Knudsen effusion cell. The evaporated sample was mixed with argon or krypton (from Messer, purity of 99.996%) before deposition. The gas flow was kept at 0.07 mmol min^{-1}, while the temperature of the Knudsen cell was optimized to get the shortest possible deposition time and keep the concentration low enough to minimize the formation of dimers in the matrix. The applied evaporation temperature was ~72 °C.

The sample–rare gas mixture was deposited onto an 8–10 K CsI or a BaF_2 window mounted on a Janis CCS-350R cold head cooled by a CTI Cryogenics 22 closed-cycle refrigerator unit. The deposition time was ca. 3–4 h ($A \approx 0.3$ for the most intense band) for FTIR and ca. 10–15 h ($A \approx 1.0$ for the most intense band) for VCD measurements.

MI-IR spectra were recorded by a Bruker IFS 55 FT-IR spectrometer equipped with a KBr beamsplitter and a DTGS detector. One thousand scans were accumulated at 1 cm^{-1} resolution. In the 1850–1450 cm^{-1} region, spectra were also recorded by a Bruker Equinox FT-IR spectrometer equipped with a KBr beamsplitter and a MCT detector. In this case 100 scans were accumulated at 2 cm^{-1} resolution. In both cases the baseline was corrected by an adjusted polynomial function, when it was necessary because of interference. The center of individual transitions in the case of unresolved bands was determined by nonlinear curve fitting.

MI-VCD spectra were recorded by a Bruker Equinox FT-IR spectrometer combined with a PMA37 VCD module and equipped with a MCT detector. Circularly polarized light was generated by the help of a KRS5 polarization filter and a ZnSe photoelastic modulator. A CdS stress plate was used for calibration. 2×13,783 scans were accumulated at 2 cm^{-1} resolution. After data processing, the baseline of the raw MI-VCD spectra was corrected by fitting a polynomial onto points with zero absorbance, as determined by the corresponding MI-IR spectrum.

3. Computational details

Geometry optimization of Ac–L-Pro–NH_2 conformers was started from structures obtained by setting the two peptide backbone dihedral angles ϕ and φ,[50] to typical values of γ_L, ε_L, and α_L conformations (see Fig. 1). The other structures generally possible in the case of other model peptides, β_{DL}, γ_D, ε_D, α_D, δ_D, and δ_L, do not exist for Ac–L-Pro–NH_2 due to the constraints of the pyrrolidine ring. Both the cis and the trans forms and the up and down puckered forms (denoted by + and −, respectively) of the pyrrolidine ring were optimized at the B3LYP/6-31G* and B3LYP/6-31++G** levels of theory. Harmonic

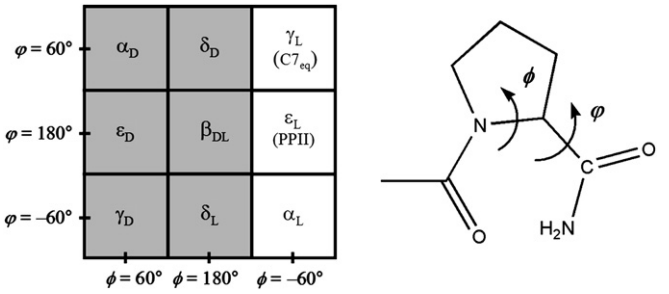

Figure 1. Qualitative conformational landscape of Ac–L-Pro–NH_2 showing the structures, which can (in white background) and cannot (in gray background) be accessed due to the constraints of the pyrrolidine ring. Besides conformational labeling notations used in former studies are given in brackets.

vibrational frequencies, infrared intensities, and rotational strengths were calculated at the B3LYP/6-31G* level of theory using the scaled quantum mechanical (SQM) force field method[51,52] with scale factors determined by Baker et al.[52] (Preoptimized SQM scale factors are not available for the 6-31++G** basis set.) Boltzmann-distributions were calculated from the B3LYP/6-31++G** Gibbs free energies. Spectra were synthesized by summing up the appropriately weighted calculated spectra of individual conformers. For spectrum simulations Lorentzian line shapes with 3 cm^{-1} half width at half height were used. All the above-mentioned calculations were performed by the PQS (Parallel Quantum Solutions) 3.2 program package.[53]

Barrier heights between conformers were calculated at the B3LYP/6-31G* and the B3LYP/6-31++G** levels of theory. These calculations were carried out by the Gaussian03 program package.[54]

Geometries in Cartesian coordinates, computed vibrational frequencies, infrared transition intensities, rotatory strengths of each conformer are available upon request.

4. Results and discussions

4.1. Computational results

In agreement with the B3LYP results of Sahai et al. we have located six minima on both the B3LYP/6-31G* and the B3LYP/6-31++G** conformational PES of Ac–L-Pro–NH_2. These minima, as they are shown in Figure 2, include two trans conformers, $t\gamma_L+$ and $t\gamma_L-$, and four cis conformers, $c\varepsilon_L+$, $c\varepsilon_L-$, $c\alpha_L+$, and $c\alpha_L-$. (Another minimum exists on the HF PES, the relatively high-energy $t\alpha_L-$ conformer.[39]) According to the calculated Gibbs free energies and Boltzmann-distributions (see Table 1) only three out of the six conformers have high enough abundance to be identifiable in the MI spectra. These are the $t\gamma_L+$, $t\gamma_L-$ and $c\alpha_L+$ forms. The computed abundance of $c\alpha_L-$ conformer is on the borderline of the detection limit. Thus, Ac–L-Pro–NH_2 has two 'low-energy' backbone conformers, namely the $t\gamma_L$ and the $c\alpha_L$.

Besides the relative Gibbs free energy the barrier height of interconversion to lower energy conformers is another factor, which can influence the existence of higher energy forms in matrices. It is often found that species with a barrier height of a few

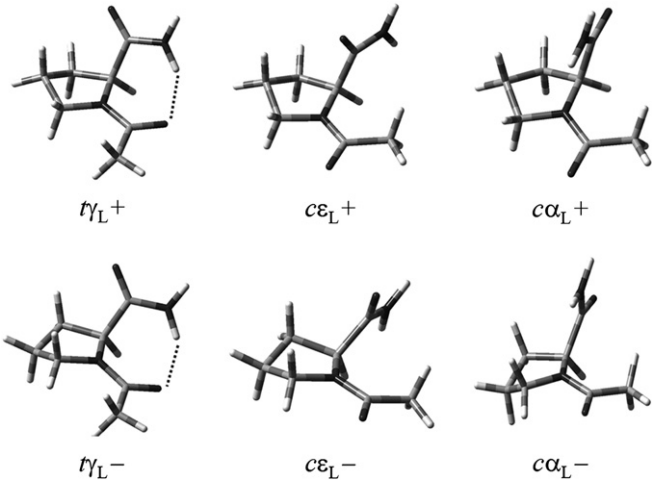

Figure 2. Conformers of Ac–L-Pro–NH_2 as obtained from geometry optimization at the B3LYP/6-31G* level of theory.

kJ mol^{-1} between them can partially or completely convert to the lower energy conformer during sticking onto the cold window.[55,56] Ramek et al.[39] have found the barrier heights from $t\gamma_L-$ to $t\gamma_L+$ to be only 2.47 and 3.44 kJ mol^{-1} at the RHF/4-31G and RHF/6-31G* levels of theory, respectively. Repeating these calculations at the B3LYP/6-31G* and B3LYP/6-31++G** levels, we have obtained somewhat larger barrier heights, 5.66 and 4.56 kJ mol^{-1}, respectively, but these values are still low enough to allow an interconversion process during freezing out the sample onto the cold surface. Hence, the $t\gamma_L-$ conformer might be absent in the matrices. On the other hand, the barrier between the cis and trans forms is ca. 60 kJ mol^{-1}, clearly preventing the interconversion of these isomers.

4.2. MI-IR spectra and conformational identification

Instead of a line-by-line assignment of the whole region we concentrate on the discussion of those regions only where the different conformers show a significantly different spectral pattern according to the theoretical calculations. The full assignment is given in Table 2. The excellent agreement between the measured and the calculated spectra made a confident assignment possible for the majority of the bands including the weakest lines, which are about ~3 times more intense than

Table 1
Calculated relative zero-point corrected energies, relative Gibbs free energies, in kJ mol^{-1}, at the temperature of sample inlet, 345 K, and relative abundances (R. A.) of the conformers of Ac–L-Pro–NH_2

Conformer	B3LYP/6-31G*			B3LYP/6-31++G**		
	ΔG^{Θ} (0 K)	ΔG^{Θ} (345 K)	R. A. (345 K)	ΔG^{Θ} (0 K)	ΔG^{Θ} (345 K)	R. A. (345 K)
$t\gamma_L+$	0	0	0.848	0.00	0	0.834
$t\gamma_L-$	5.41	5.08	0.144	5.22	5.16	0.138
$c\alpha_L+$	17.63	15.03	0.004	13.25	10.80	0.019
$c\alpha_L-$	21.07	17.34	0.002	16.47	13.79	0.007
$c\varepsilon_L+$	27.12	19.77	0.001	23.55	18.12	0.002
$c\varepsilon_L-$	29.46	22.75	0.000	25.48	20.66	0.001

Table 2
Calculated (SQM B3LYP/6-31G*) and experimental vibrational frequencies in cm^{-1} of Ac–L-Pro–NH_2

Assignment[a]	Calcd	Ar	Kr
$c\alpha_L+$ ν_1 (amide A *asym.*)	3601	3546	3539
$t\gamma_L+$ ν_1 (amide A *asym.*)	3543	3502	3497
$c\alpha_L+$ ν_2 (amide A *sym.*)	3465	3436	3429
$t\gamma_L+$ $2\nu_{13}$ (overtone)	—	3427	3421
$t\gamma_L+$ $\nu_{13}+\nu_{14}$ (combination band)	—	3370	3369
$t\gamma_L+$ ν_2 (amide A *sym.*)	3342	3313	3305
$t\gamma_L+$ $2\nu_{14}$ (Fermi resonance with ν_4)	—	3287[b]	3284[b]
$t\gamma_L+$ $\nu_{14}+\nu_{15}$ (combination band)	—	3227	3222
$t\gamma_L+$ $2\nu_{15}$ (overtone)	—	3146	3139
$t\gamma_L+$ ν_3 ($\nu_{asym}CH_3$)	3041	3025	3033[b]
$t\gamma_L+$ ν_4 ($\nu_{asym}CH_2$)	3021	3021	3018
$t\gamma_L+$ ν_5 ($\nu_{asym}CH_2$)	2999	2991	2983
n.a.	—	2979	2973
$t\gamma_L+$ ν_6 ($\nu_{asym}CH_2$)	2982	2964	2961
$t\gamma_L+$ ν_7 (νCH)	2955	2947[c]	2943[c]
$t\gamma_L+$ ν_8 ($\nu_{sym}CH_2$)	2951	2947[c]	2943[c]
$t\gamma_L+$ ν_9 ($\nu_{sym}CH_2$)	2947	2947[c]	2943[c]
$t\gamma_L+$ ν_{10} ($\nu_{sym}CH_2$)	2932	2934	2931
$t\gamma_L+$ ν_{11} ($\nu_{sym}CH_3$)	2922	2920[b]	2918[b]
n.a.	—	2900[b]	2898[b]
n.a.	—	2885[b]	2882[b]
$t\gamma_L+$ ν_{12} ($\nu_{sym}CH_2$)	2890	2877	2874
$c\alpha_L+$ ν_{13} (C-term. amide I)	1737	1737	1735
$t\gamma_L+$ ν_{13} (N-term. amide I)	1730	1716	1713
Aggregate or complex[d]	—	1703[b]	1704[b]
$c\alpha_L+$ ν_{14} (N-term. amide I)	1701	1687	1684
$t\gamma_L+$ ν_{14} (C-term. amide I)	1665	1654	1652
Aggregate or complex[d]	—	1642[b]	1638[b]
$t\gamma_L+$ ν_{15} (amide II)	1598	1578	1576
$c\alpha_L+$ ν_{15} (amide II)	1575	1568	1559
$t\gamma_L+$ ν_{16} ($\beta_{sym}CH_2$)	1484	1480	1480
$t\gamma_L+$ ν_{17} ($\beta_{sym}CH_2$)	1461	1459	1457
$t\gamma_L+$ ν_{18} ($\delta_{asym}CH_3$)	1442	1443[b,c]	1441[b,c]
$t\gamma_L+$ ν_{19} ($\beta_{sym}CH_2$)	1441	1443[b,c]	1441[b,c]
$t\gamma_L+$ ν_{20} ($\delta_{asym}CH_3$)	1424	1438	1436
$t\gamma_L+$ ν_{21} (νCN+$\delta_{sym}CH_3$)	1402	1418	1416
$t\gamma_L+$ ν_{22} (amide III)	1367	1387	1386
$c\alpha_L+$ ν_{21} (amide III)	1374	1354	1353
$t\gamma_L+$ ν_{23} ($\delta_{sym}CH_3$)	1341	1341[c]	1339[c]
$t\gamma_L+$ ν_{24} ($\delta_{sym}CH_2$)	1339	1341[c]	1339[c]
$t\gamma_L+$ ν_{25} ($\delta_{sym}CH_2$)	1321	1322	1321
$t\gamma_L+$ ν_{26} ($\delta_{sym}CH_2$)	1312	1314	1313
$t\gamma_L+$ ν_{27} (δ $C^{\alpha}H$)	1291	1292	1291
$t\gamma_L+$ ν_{28} (δ $C^{\alpha}H$)	1264	1271	1271
$t\gamma_L+$ ν_{29} ($\gamma_{asym}CH_2$)	1241	1248	1249
$t\gamma_L+$ ν_{30} ($\gamma_{asym}CH_2$)	1187	1189[c]	1188[c]
$t\gamma_L+$ ν_{31} ($\gamma_{asym}CH_2$)	1178	1189[c]	1188[c]
$t\gamma_L+$ ν_{32} ($\gamma_{asym}CH_2$)	1149	1159	1159
$t\gamma_L+$ ν_{33} ($\beta_{asym}NH_2+\beta_{asym}CH_2$)	1119	1120	1118
$t\gamma_L+$ ν_{34} ($\beta_{asym}NH_2+\beta_{asym}CH_2$)	1081	1083	1083
$t\gamma_L+$ ν_{35} ($\beta_{asym}NH_2$)	1120	1085	1085
$t\gamma_L+$ ν_{36} ($\delta_{asym}CH_3$)	1026	1036[c]	1035[c]
$t\gamma_L+$ ν_{37} ($\delta_{asym}CH_3$)	1016	1036[c]	1035[c]
$t\gamma_L+$ ν_{38}	975	993	993
$t\gamma_L+$ ν_{39}	939	960	959
n.a.	—	924	923
$t\gamma_L+$ ν_{40} ($\beta_{asym}CH_2$)	904	908[c]	908[c]
$t\gamma_L+$ ν_{41} ($\beta_{asym}CH_2$)	894	908[c]	908[c]
$t\gamma_L+$ ν_{42} ($\beta_{asym}CH_2$)	862	877[b]	876[b]
$t\gamma_L+$ ν_{43}	853	869	868
$t\gamma_L+$ ν_{44}	772	791	791
$t\gamma_L+$ ν_{45} (amide V)	736	721	717
$t\gamma_L+$ ν_{46}	660	660	660
$t\gamma_L+$ ν_{47} (C-term. amide VI)	642	639	637
$t\gamma_L+$ ν_{48}	612	613	612
$t\gamma_L+$ ν_{49} (N-term. amide VI)	592	603	602
$t\gamma_L+$ ν_{50}	553	556	555
$t\gamma_L+$ ν_{51} ($\gamma_{sym}NH_2$)	514	512	510
$t\gamma_L+$ ν_{52} ($\gamma_{sym}NH_2$)	483	466	465
$t\gamma_L+$ ν_{53} ($\gamma_{sym}NH_2$)	433	434	432

[a] The assignments are tentative in the 1400–1200 cm^{-1} region.
[b] Shoulder.
[c] Unresolved lines.
[d] See text for details.

the noise level. Only five very low-intensity bands were not assigned and are labeled by n.a. in Table 2.

It is evident already at the first look (see Figs. 3–5) that the dominant features of the MI-IR spectra can be assigned to the most abundant $t\gamma_L+$ conformer. The next low-energy form is that of the $t\gamma_L+$ conformer. Comparing the computed spectra of the $t\gamma_L+$ and $t\gamma_L-$ conformers, the most significant difference is found in the 425–575 cm^{-1} region. Here (see Fig. 3)

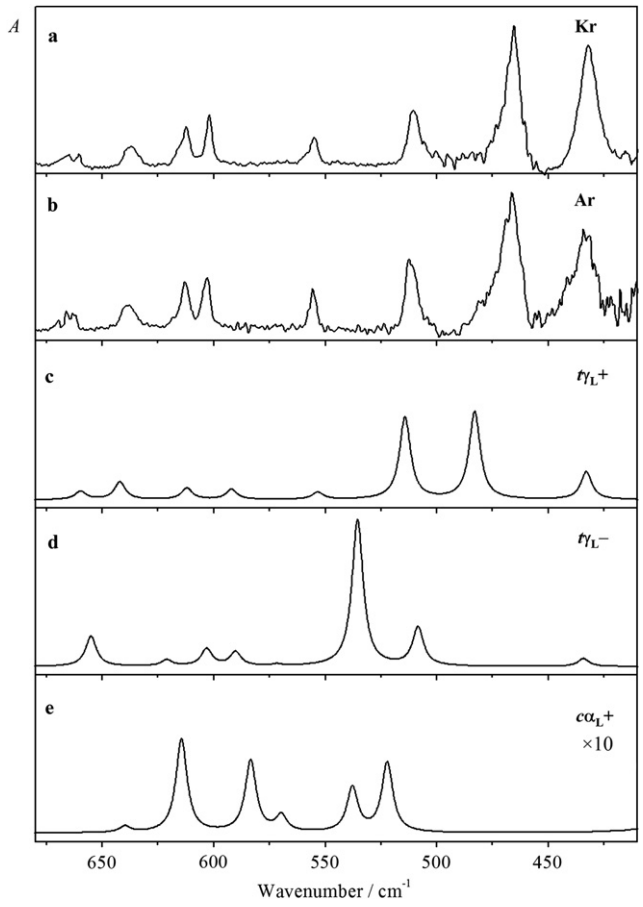

Figure 3. Low-frequency region of IR spectra of Ac–L-Pro–NH_2 as observed in (a) Kr matrix, (b) Ar matrix, and the calculated IR spectra of individual conformers of (c) $t\gamma_L+$, (d) $t\gamma_L-$, and (e) $c\alpha_L+$. The intensity of the calculated spectrum of $c\alpha_L+$ is multiplied by a factor of 10 as compared to the two trans conformers.

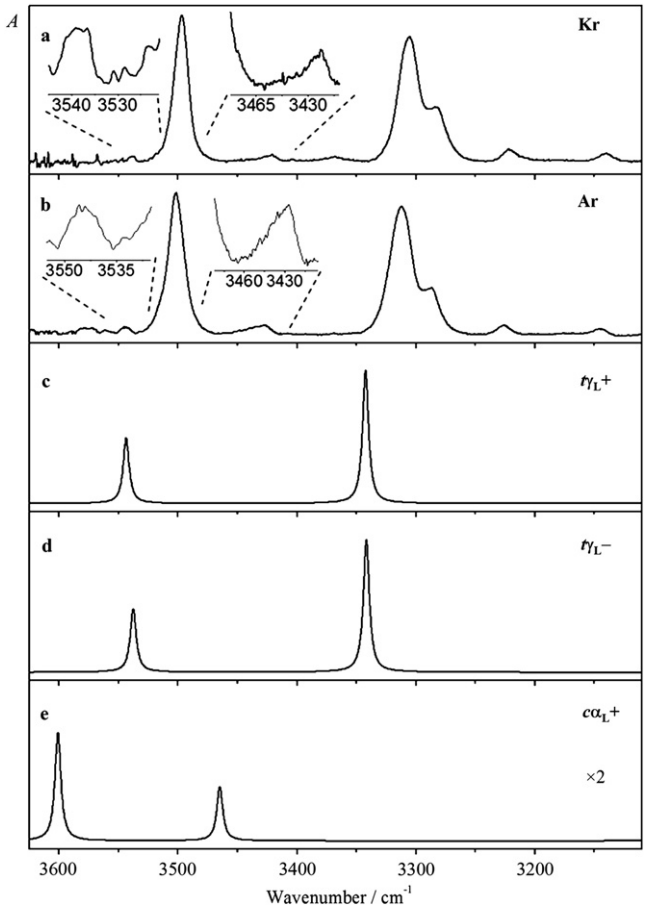

Figure 4. Amide A region of IR spectra of Ac–L-Pro–NH_2 as observed in (a) Kr matrix, (b) Ar matrix, and the calculated IR spectra of individual conformers of (c) $t\gamma_L+$, (d) $t\gamma_L-$, and (e) $c\alpha_L+$. Inserts show the peaks enlarged, which are assigned to the $c\alpha_L+$ conformer. The intensity of the calculated spectrum of $c\alpha_L+$ is multiplied by a factor of 2 as compared to the two trans conformers.

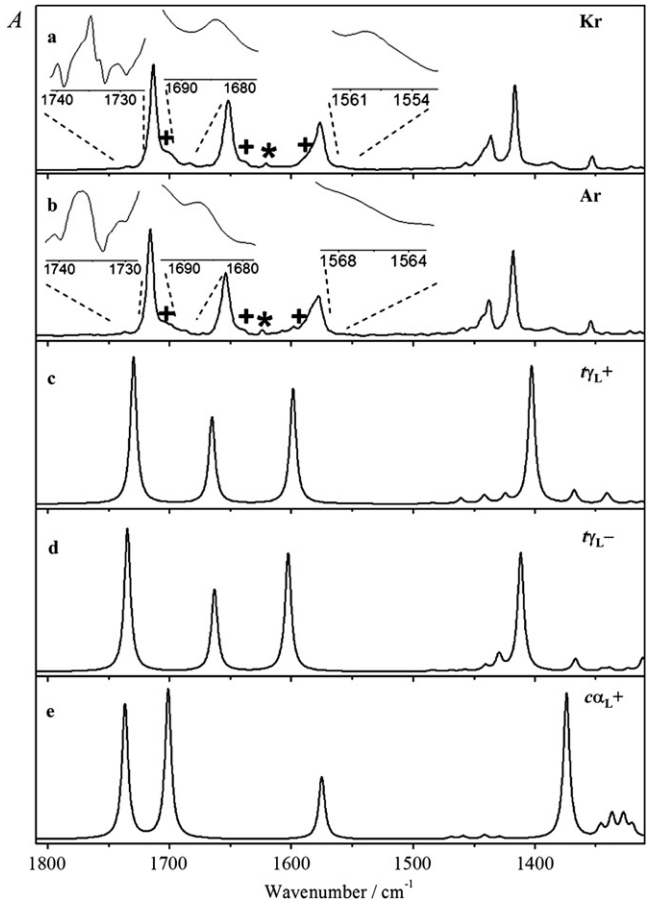

Figure 5. Amide I and II regions of IR spectra of Ac–L-Pro–NH_2 as observed in (a) Kr matrix, (b) Ar matrix, and the calculated IR spectra of individual conformers of (c) $t\gamma_L+$, (d) $t\gamma_L-$, and (e) $c\alpha_L+$. Inserts show the peaks enlarged, which are assigned to the $c\alpha_L+$ conformer. Broad features due to aggregates and/or complexes with water are labeled by a plus sign. Water traces are marked by asterisk.

four transitions of the $t\gamma_L+$ are expected to show up according to the calculations. These are clearly visible both in the Ar and Kr matrix spectra. For the $t\gamma_L-$ conformer also four transitions are expected to be present in this region. Among these transitions the most intense one at 535 cm^{-1} is well separated from those of the $t\gamma_L+$ conformer's features. However, this intense transition is completely missing from the MI-IR spectra. Not only this region, but each line of the whole-range spectra could be entirely assigned in the absence of the $t\gamma_L-$ conformer. This result justifies the existence of a low barrier conversion path from $t\gamma_L-$ to $t\gamma_L+$ conformer.

As it is expected, the spectra of cis and trans forms show the largest differences in the transitions of amide vibrational modes. Hence, we analyzed the amide A and amide I and II modes in order to search for the $c\alpha_L+$ conformer. The amide A region should be examined carefully, since our former matrix isolation study on Ac–Gly–NHMe and Ac–L-Ala–NHMe[57] has shown that besides fundamental amide A transitions Fermi resonances and overtones of amide I modes can clearly appear in this region. After considering all fundamentals, possible Fermi resonances and overtones of the $t\gamma_L+$ conformer (see Table 2), a low-intensity band at 3546/3539 cm^{-1} in Ar/Kr still remains unassigned in this region (see Fig. 4). This band appears at ca. 40–50 cm^{-1} higher frequency than the highest frequency transition of the $t\gamma_L+$ conformer. Since the calculations predict the highest frequency fundamental of the $c\alpha_L+$ conformer 58 cm^{-1} higher than that of the $t\gamma_L+$ form (see Table 2), the band observed at 3546/3539 cm^{-1} can be assigned to the asymmetric amide A mode of the $c\alpha_L+$ conformer. The symmetric amide A transition of $c\alpha_L+$ is calculated to be 3465 cm^{-1}. In the amide A region of the MI-IR spectra the only band, which does not have a symmetric line shape is the one between 3400 and 3440 cm^{-1}. As it can be seen in the insets of Figure 4 two bands can be fitted under this peak. The lower-frequency one is assigned the ν_{13} overtone of the $t\gamma_L+$ conformer, while the band at higher frequency to the symmetric amide A transition of $c\alpha_L+$ conformer (see Table 2).

The low-intensity transitions of the $c\alpha_L+$ isomer can also be identified in the amide I and II regions (see Fig. 5). This 1450–1750 cm^{-1} region is dominated by the three intense transitions of the $t\gamma_L+$ conformer. In addition to these bands, traces of water (indicated by an asterisk in Fig. 5) and broad bands (indicated by plus sign in Fig. 5) due to aggregates or

complexes with traces of water can be identified. (The intensity of these broad features varied slightly upon the conditions of deposition.) As it was found in the amide A region, the remaining low-intensity bands at 1737/1735, 1687/1684, and 1568/1559 cm^{-1} in Ar/Kr can be assigned in good agreement with the calculated transitions, 1737, 1701, and 1575 cm^{-1}, to the $c\alpha_L+$ conformer.

In conclusion the $t\gamma_L+$ form and trace amounts of the $c\alpha_L+$ conformer can be identified in the MI-IR spectra. All the features of the spectra can be assigned to either of these species. In accordance with the theoretical predictions $c\varepsilon_L+$ and $c\varepsilon_L-$ conformers are not populated enough at the temperature of sample inlet, 72 °C, to be visible in the MI-IR spectra, while the $t\gamma_L-$ conformer converts to the $t\gamma_L+$ form upon sticking onto the cold surface. Because of its low predicted abundance and the low-energy barrier[39] to its ring-puckered counterpart, the $c\alpha_L-$ form has not been observed either. According to this the conformational ratio of the $t\gamma_L+$ and the $c\alpha_L+$ conformers in the matrices can be calculated by summing up the Boltzmann-weights of the individual + and − conformers. In order to obtain a calculated spectrum these summed factors, 0.972 and 0.026 for $t\gamma_L+$ and $c\alpha_L+$, respectively, were used to weigh the intensities of the individual conformer spectra. As can be seen in Figure 6 the spectrum obtained this way agrees very well with the MI-IR spectra.

4.3. MI-VCD spectra

It has been shown before that the MI-VCD spectrum of molecules capable of strong interactions can be understood much easier than the spectra recorded in solutions, where the intermolecular interactions can significantly alter the spectra.[57,58] As it can be seen in Figure 7 an excellent agreement was found between MI-VCD spectra and calculations in the investigated 1775−1550 cm^{-1} region.

It is interesting to compare the MI-VCD spectra to the VCD spectra of Ac−L-Pro−ND_2 recorded in D_2O and deuterated alcohols.[15] In those protic solvents, in agreement with the

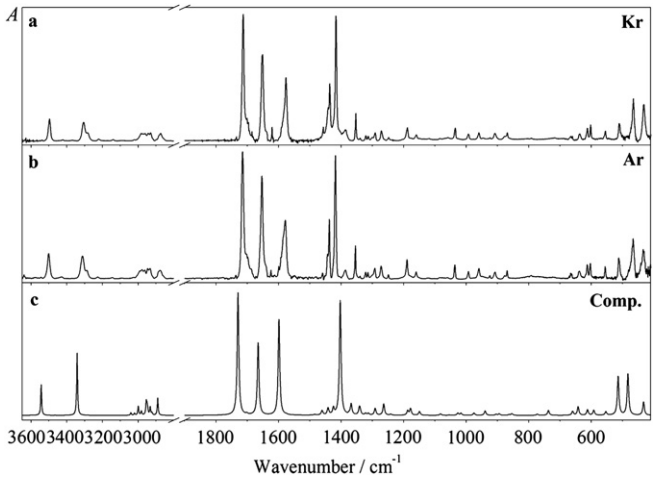

Figure 6. Whole-range MI-IR spectra of Ac−L-Pro−NH_2 recorded in (a) Kr matrix and in (b) Ar matrix, and (c) computed IR spectra obtained by appropriate weighting (see text for details) of the individual conformer spectra.

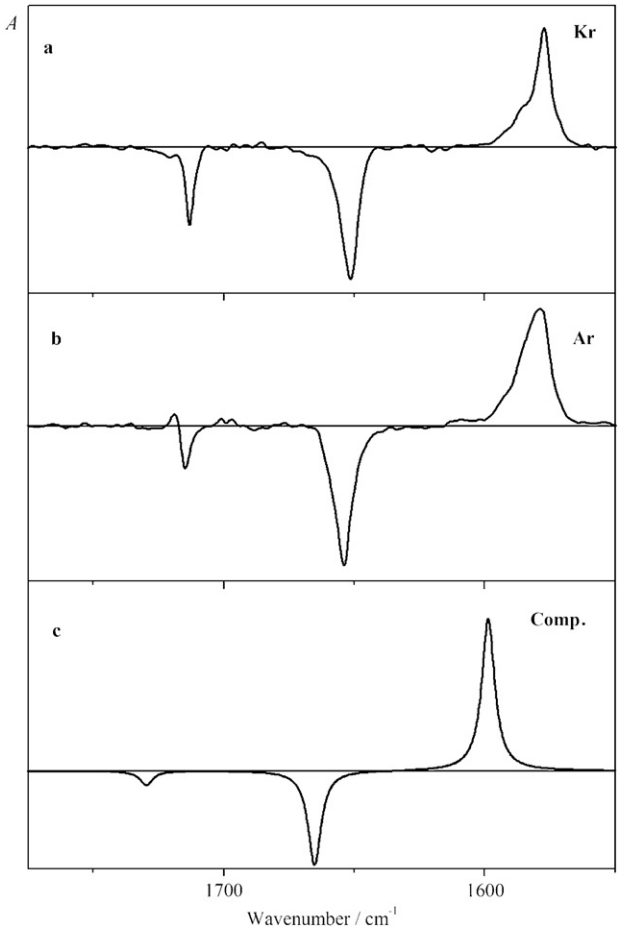

Figure 7. 1775−1550 cm^{-1} region of MI-VCD spectra of Ac−L-Pro−NH_2 recorded in (a) Kr matrix and in (b) Ar matrix, and (c) computed VCD spectra obtained by appropriate weighting (see text for details) of the individual conformer spectra. The $\Delta A=0$ level is given by a thin solid line in each spectrum.

MI-VCD spectra, the low-frequency amide I mode appears as a negative band between 1608 and 1634 cm^{-1}. On the other hand the sign of the high-frequency amide I transition, between 1646 and 1668 cm^{-1}, is positive. This is opposite to both the MI-IR observations and the calculations for the $t\gamma_L+$ conformer. Moreover, none of the six conformers of Ac−L-Pro−NH_2 has a positive rotatory strength predicted for the high-frequency amide I transition. This indicates that the structure of Ac−L-Pro−NH_2 in aqueous or alcoholic solvents is different from the possible structures of the isolated molecule and/or the solvent−solute interaction significantly changes the rotatory strengths.

5. Summary

In this paper we have presented the MI-IR and MI-VCD spectra of Ac−L-Pro−NH_2 in Ar and Kr matrices. The analysis of spectra revealed that two backbone conformers, the major $t\gamma_L+$ and the minor $c\alpha_L+$ forms exist in observable amounts (>1%). Theoretical calculations predict an additional low-energy conformer, $t\gamma_L-$, but that conformer converts to the $t\gamma_L+$ structure through a low-energy path when freezing onto the cold surface. A similar conversion is expected between

the + and − forms of the minor conformers. The computed spectra based on this conformational model show a very good agreement with the measurements. Our results are in accord with former IR and NMR investigation of Ac−L-Pro−NH_2 solutions, which showed that in apolar solvents the trans forms are dominant, and the ratio of the cis forms increases by increasing solvent polarity. The observation that the proline diamide has hardly any alternative conformer than $t\gamma_L(+/-)$ not only supports the general view on the elevated rigidity of this amino acid residue, but also explains how it can be an effective α-helix breaker and a β-edge distorter preventing β-proteins to aggregate.

A future direction of our investigations is the analysis of the spectra of the water complexes of Ac−L-Pro−NH_2, which can possibly reveal conformational change upon complexation. In the present study it has been shown that the isolated Ac−L-Pro−NH_2 adopts only one trans form, $t\gamma_L$, which agrees with the well-known α-helix and β-sheet breaking nature of proline. It is an interesting question, however, whether the $t\alpha_L-$ form can be stabilized by complexed water molecules. In addition to MI-IR experiments we plan to investigate these complexes by MI-VCD spectroscopy as well, which could help to understand the VCD spectra observed in D_2O and deuterated alcohols.

Acknowledgements

This work was funded by the Hungarian Ministry of Education (FKFP 0131/2001), the Economic Competitiveness Operational Program GVOP-KMA (GVOP-3.2.1-2004-04-0010/3.0 and GVOP-3.2.1-2004-04-0345/3.0), and the Hungarian Scientific Research Fund (OTKA F042722, T047186, and T049792). G.T. was supported by the János Bolyai Research Scholarship of the Hungarian Academy of Sciences.

References and notes

1. Wedemeyer, W. J.; Welker, E.; Scheraga, H. A. *Biochemistry* **2002**, *41*, 14637.
2. Hudaky, I.; Baldoni, H. A.; Perczel, A. *J. Mol. Struct. (THEOCHEM)* **2002**, *582*, 233.
3. Mizushima, S.; Shimanouchi, T.; Tsuboi, M.; Sugita, T.; Kurosaki, K.; Mataga, N.; Souda, R. *J. Am. Chem. Soc.* **1952**, *74*, 4639.
4. Tsuboi, M.; Shimanouchi, T.; Mizushima, S. *J. Am. Chem. Soc.* **1959**, *81*, 1406.
5. Avignon, M.; Huong, P. V.; Lascombe, J.; Marraud, M.; Neel, J. *Biopolymers* **1969**, *8*, 69.
6. Madison, V.; Schellman, J. *Biopolymers* **1970**, *9*, 65.
7. Madison, V.; Schellman, J. *Biopolymers* **1969**, *9*, 511.
8. Stimson, E. R.; Zimmerman, S. S.; Scheraga, H. A. *Macromolecules* **1977**, *10*, 1049.
9. Koyama, Y.; Uchida, H.; Oyama, S.; Iwaki, T.; Harada, K. *Biopolymers* **1977**, *16*, 1795.
10. Madison, V.; Kopple, K. D. *J. Am. Chem. Soc.* **1980**, *102*, 4855.
11. Liang, G.-B.; Rito, C. J.; Gellman, S. H. *Biopolymers* **1992**, *32*, 293.
12. Akiyama, M.; Phtani, T.; Furuta, Y.; Watanabe, E. *Spectrochim. Acta* **1994**, *50A*, 1675.
13. Miyazawa, M.; Inouye, K.; Hayakawa, T.; Kyogoku, Y.; Sugeta, H. *Appl. Spectrosc.* **1996**, *50*, 644.
14. Lee, K.-K.; Hahn, S.; Oh, K.-I.; Choi, J.-S.; Joo, C.; Lee, H.; Han, H.; Cho, M. *J. Phys. Chem. B* **2006**, *110*, 18834.
15. Oh, K.-I.; Han, J.; Lee, K.-K.; Hahn, S.; Han, H.; Cho, M. *J. Phys. Chem. A* **2006**, *110*, 13355.
16. Madison, V.; Delaney, N. G. *Biopolymers* **1983**, *22*, 869.
17. Asplund, M. C.; Zanni, M. T.; Hochstrasser, R. M. *Proc. Natl. Acad. Sci. U.S.A.* **2000**, *97*, 8219.
18. Zanni, M. T.; Ge, N.-H.; Kim, Y. S.; Hochstrasser, R. M. *Proc. Natl. Acad. Sci. U.S.A.* **2001**, *98*, 11265.
19. Zanni, M. T.; Gnanakaran, S.; Stenger, J.; Hochstrasser, R. M. *J. Phys. Chem. B* **2001**, *105*, 6520.
20. Ge, N.-H.; Zanni, M. T.; Hochstrasser, R. M. *J. Phys. Chem. A* **2002**, *106*, 962.
21. Rubtsov, I. V.; Hochstrasser, R. M. *J. Phys. Chem. B* **2002**, *106*, 9165.
22. Rubtsov, I. V.; Wang, J.; Hochstrasser, R. M. *J. Phys. Chem. B* **2003**, *107*, 3384.
23. Park, J.; Hochstrasser, R. M. *Chem. Phys.* **2006**, *323*, 78.
24. Sul, S.; Karaiskaj, D.; Jiang, Y.; Ge, N.-H. *J. Phys. Chem. B* **2006**, *110*, 19891.
25. Torchia, D. A. *Macromolecules* **1971**, *4*, 440.
26. Dorman, D. E.; Bovey, F. A. *J. Org. Chem.* **1973**, *38*, 2379.
27. Higashimija, T.; Tasumi, M.; Miyazawa, T. *Biopolymers* **1977**, *16*, 1259.
28. Siemion, I. Z.; Picur, B. *Biophys. Chem.* **1988**, *31*, 71.
29. Taylor, C. M.; Hardre, R.; Edwards, P. J. B.; Park, J. H. *Org. Lett.* **2003**, *5*, 4413.
30. Madison, V. *Biopolymers* **1977**, *16*, 2671.
31. Rosas, R. I.; Cooper, C.; Laane, J. *J. Phys. Chem.* **1990**, *94*, 1830.
32. Koca, J.; Kriz, Z.; Carlsen, P. H. J. *J. Mol. Struct. (THEOCHEM)* **1994**, *306*, 157.
33. McDonald, Q.; Still, W. C. *J. Org. Chem.* **1996**, *61*, 1385.
34. Momany, F. A.; McGuire, R. F.; Burgess, A. W.; Scheraga, H. A. *J. Phys. Chem.* **1975**, *79*, 2362.
35. Zimmerman, S. S.; Pottle, M. S.; Némethy, G.; Scheraga, H. A. *Macromolecules* **1977**, *10*, 1.
36. Vasquez, M.; Némethy, G.; Scheraga, H. A. *Macromolecules* **1983**, *16*, 1043.
37. Némethy, G.; Gibson, K. D.; PAlmer, K. A.; Yoon, C. N.; Paterlini, G.; Zagari, A.; Rumsey, S.; Scheraga, H. A. *J. Phys. Chem.* **1992**, *96*, 6472.
38. Fischer, S.; Dunbrack, R.; Karplus, M. *J. Am. Chem. Soc.* **1994**, *116*, 11931.
39. Ramek, M.; Kelterer, A.-M.; Teppen, B. J.; Schafer, L. *J. Mol. Struct.* **1995**, *352*, 59.
40. Kang, Y. K. *J. Phys. Chem.* **1996**, *100*, 11589.
41. Jhon, J. S.; Kang, Y. K. *J. Phys. Chem.* **1999**, *103*, 5436.
42. Kang, Y. K.; Park, H. S. *J. Mol. Struct. (THEOCHEM)* **2002**, *593*, 55.
43. Oldziej, S.; Kozlowska, U.; Liwo, A.; Scheraga, H. A. *J. Phys. Chem. A* **2003**, *107*, 8035.
44. Kang, Y. K.; Choi, H. Y. *Biophys. Chem.* **2004**, *111*, 135.
45. Kang, Y. K. *J. Mol. Struct. (THEOCHEM)* **2004**, *675*, 37.
46. Kang, Y. K. *J. Phys. Chem. B* **2004**, *108*, 5463.
47. Sahai, M. A.; Kehoe, T. A. K.; Koo, J. C. P.; Setiadi, D. H.; Chass, G. A.; Viskolcz, B.; Penke, B.; Pai, E. F.; Csizmadia, I. G. *J. Phys. Chem. A* **2005**, *109*, 2660.
48. Kang, Y. K. *J. Phys. Chem. B* **2006**, *110*, 21338.
49. Rankin, K. N.; Boyd, R. J. *J. Phys. Chem. A* **2002**, *106*, 11168.
50. Császár, A. G.; Perczel, A. *Prog. Biophys. Mol. Biol.* **1999**, *71*, 243.
51. Pulay, P.; Fogarasi, G.; Pongor, G.; Boggs, J. E.; Vargha, A. *J. Am. Chem. Soc.* **1983**, *105*, 7037.
52. Baker, J.; Jarzecki, A. A.; Pulay, P. *J. Phys. Chem. A* **1998**, *102*, 1412.
53. PQS version 3.2; Parallel Quantum Solutions: 2013 Green Acres Road, Fayetteville, AR 72703, 2005.
54. Frisch, M. J.; Trucks, G. W.; Schlegel, H. B.; Scuseria, G. E.; Robb, M. A.; Cheeseman, J. R.; Montgomery, J. A., Jr.; Vreven, T.; Kudin, K. N.; Burant, J. C.; Millam, J. M.; Iyengar, S. S.; Tomasi, J.; Barone, V.; Mennucci, B.; Cossi, M.; Scalmani, G.; Rega, N.; Petersson, G. A.; Nakatsuji, H.; Hada, M.; Ehara, M.; Toyota, K.; Fukuda, R.; Hasegawa, J.; Ishida, M.; Nakajima, T.; Honda, Y.; Kitao, O.; Nakai, H.; Klene, M.; Li, X.; Knox, J. E.; Hratchian, H. P.; Cross, J. B.; Adamo, C.; Jaramillo, J.; Gomperts, R.; Stratmann, R. E.; Yazyev, O.; Austin, A. J.; Cammi, R.; Pomelli, C.; Ochterski, J. W.; Ayala, P. Y.; Morokuma, K.; Voth, G. A.; Salvador, P.; Dannenberg, J. J.; Zakrzewski, V. G.; Dapprich, S.; Daniels, A. D.; Strain, M. C.; Farkas, O.; Malick, D. K.; Rabuck,

A. D.; Raghavachari, K.; Foresman, J. B.; Ortiz, J. V.; Cui, Q.; Baboul, A. G.; Clifford, S.; Cioslowski, J.; Stefanov, B. B.; Liu, G.; Liashenko, A.; Piskorz, P.; Komaromi, I.; Martin, R. L.; Fox, D. J.; Keith, T.; Al-Laham, M. A.; Peng, C. Y.; Nanayakkara, A.; Challacombe, M.; Gill, P. M. W.; Johnson, B.; Chen, W.; Wong, M. W.; Gonzalez, C.; Pople, J. A. *Gaussian 03, Revision C.02*; Gaussian: Wallingford CT, 2004.

55. Reva, I. D.; Stepanian, S. G.; Adamowicz, L.; Fausto, R. *Chem. Phys. Lett.* **2003**, *374*, 631 and references therein.
56. Mátyus, E.; Magyarfalvi, G.; Tarczay, G. *J. Phys. Chem. A* **2007**, *111*, 450.
57. Pohl, G.; Perczel, A.; Vass, E.; Magyarfalvi, G.; Tarczay, G. *Phys. Chem. Chem. Phys.* **2007**, *9*, 4698.
58. Tarczay, G.; Magyarfalvi, G.; Vass, E. *Angew. Chem., Int. Ed.* **2006**, *45*, 1775.